Journal of Membrane Science & Research

journal homepage: www.msrjournal.com

Research Paper

Elucidating the Role of Bulky Fluorinated Segments in Thermally Rearranged Copolymers and Polymer Blends for Gas Separation

Joon Yong Bae [1], Won Hee Lee [1,2], Hae Min Kim [1], Young Jun Lee [1], Young Moo Lee [1,*]

[1] *Department of Energy Engineering, College of Engineering, Hanyang University, Seoul, 04763, Republic of Korea*
[2] *School of Chemical & Biomolecular Engineering, Georgia Institute of Technology, 311 Ferst Drive NW, Atlanta, Georgia 30332, United States*

Article info

Received 2021-10-11
Revised 2021-12-20
Accepted 2021-12-20
Available online 2021-12-20

Keywords

Thermal rearrangement
Hexafluoroisopropylidene
Copolymer
Polymer blend
Microporosity
Gas separation

Highlights

- A series of thermally rearranged (TR) polymers with different amounts of fluorinated units was synthesized for gas separation.
- Both copolymerization and polymer blending methods were used for controlling the fluorine content.
- Gas permeability increased with increasing amount of hexafluoroisopropylidene moieties in the TR polymers.
- TR polymer blend membranes exhibited higher gas permeability and comparable selectivity compared to the TR copolymers.

Graphical abstract

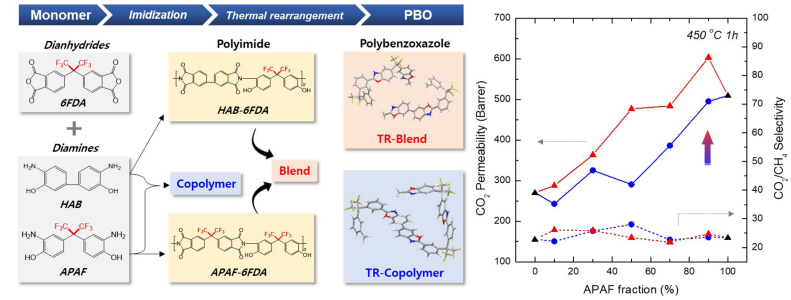

Abstract

Thermally rearranged (TR) polymers have shown outstanding gas transport properties due to their rigid polymer structure. Additionally, bulky fluorinated substituents, such as hexafluoroisopropylidene, have enhanced the gas permeability of TR polymers. Herein, the role of the fluorinated content in TR polymers in terms of their microporous structure and gas separation performance was investigated by controlling fluorine content via either a copolymerization or a polymer blending approach. A series of TR copolymers and TR polyblends were successfully prepared via post-fabrication of their precursors of copolyimides or polyimide blends, respectively. All of the precursor polyimides exhibited an imide-to-benzoxazole thermal cyclization reaction around 400 °C, regardless of the fluorinated unit contents and polymer preparation methods. The microporosity and gas permeability of the polymers were enhanced by TR conversion and the presence of hexafluoroisopropylidene moieties due to the rigid polymer backbone and the bulky units. Furthermore, the TR polymer blends exhibited distinctive thermomechanical properties with two distinct glass transition temperatures and improved gas transport properties compared to the corresponding TR copolymers synthesized from the same starting monomers. In this study, the TR polymer blend containing 90% fluorinated diamine, TR-Blend-AH91, showed the highest gas permeability ($P(CO_2)$ = 603 Barrer) among the TR polymers in this work.

1. Introduction

Membrane-based gas separation has received significant attention from academia and industry due to its advantages, such as scalability, low footprint, and simple operation [1-4]. Membrane systems separate gas molecules mainly based on differences in their size without critical physical or chemical reactions, and therefore, use less energy for gas separation compared to other classical separation processes such as cryogenic distillation or pressure swing adsorption, which require energy-intensive phase transitions [5]. Polymers have been regarded as the most feasible candidates for gas separation membranes among other materials, including carbons, metals, or ceramics, because they are easy to be produced in appropriate geometries, relatively inexpensive, and show acceptable thermal and mechanical properties for gas separation [6,7]. However, the trade-off between gas permeability and selectivity remains a major challenge for polymer membranes for gas separation [8]. To overcome this issue, many studies have been done on polymer structure designs to endow the membranes with free volume elements [9-20].

After polytetrafluoroethylene (PTFE) was developed by Plunkett in 1941 [21], perfluoropolymers have shown great potential for gas separations with

* Corresponding author: ymlee@hanyang.ac.kr (Y.M. Lee)

DOI: 10.22079/JMSR.2021.540703.1505

outstanding gas permeability [22,23]. Moreover, the development of solvent processable commercial perfluoropolymers such as Teflon® AF (DuPont), Hyflon® AD (Solvay), and Cytop (Asahi glass) accelerated the use of perfluoropolymers in membrane applications [24]. Dr. Yampolskii was one of the great contributors to perfluoropolymers for gas separations over the last 30 years. His work elucidated gas sorption, diffusion, and permeation in perfluorinated polymer matrices and introduced many novel perfluoropolymers for gas transport [25-29]. Based on his huge achievements, fluorinated moieties have been incorporated into other polymer backbones, such as polycarbonates (PC) [30], polyimides (PI) [31,32], and microporous polymers [33] to improve their gas transport.

Thermally rearranged (TR) polymers, which were first reported by *Lee* et al. in 2007, are a new class of microporous polymers that have outstanding gas transport properties [16,34-40]. Their microporosity comes from post-fabrication thermal treatments of polyimides with ortho-positioned functional groups. For instance, when an *o*-hydroxyl polyimide (HPI) is thermally rearranged into a polybenzoxazole (TR-PBO), the increasing polymer rigidity frustrates chain motions and therefore induces additional free volume in the polymer matrix [41]. TR polymer membranes have been extensively investigated, focusing on the chemical design of high-performance TR polymers [42-48] and their manufacture into various membrane geometries from flat-sheet films to hollow fibers for practical gas separation applications [49-53]. Notably, fluorinated units have been incorporated into TR backbones in an attempt to enhance their gas transport behavior. Our latest work on TR polymer membranes has shown the inclusion of bulky fluorinated segments, such as hexafluoroisopropylidene (CF_3-C-CF_3), in semi-interpenetrating polymer networks of TR polymers greatly improved gas separation performance for carbon capture and olefin/paraffin separation applications [54,55]. Therefore, studies on the role of the fluorinated moiety in TR polymers remain important for gas separation membranes.

In this study, we precisely controlled the composition of the fluorinated and non-fluorinated starting monomers, which were APAF and HAB, respectively, in a series of HPIs and TR polymers by two different polymer preparation methods: *i) Copolymerization*, and *ii) Polymer blending*. These multicomponent polymer systems have been widely preferred over the use of mere homopolymers to improve performance or lower material costs [46,56-61]. The objective of this work is to demonstrate the effect of the fluorinated moiety in the TR backbone on thermal properties, microporosity, and gas transport behavior in two different multicomponent polymer systems. To the best of our knowledge, this work is the first report of a direct comparison of TR copolymers and TR polyblends for membrane gas separation.

2. Material and methods

2.1. Materials

4,4′-(Hexafluoroisopropylidene)diphthalic anhydride (6FDA) and 2,2-bis(3-amino-4-hydroxyphenyl)hexafluoropropane (APAF) were purchased from Daikin Industries, Ltd. (Osaka, Japan). Dianhydride (6FDA) was kept in a vacuum oven at 100 °C at least one day prior to synthesis. 3,3′-dihydroxyl-4,4′-diaminobiphenyl (HAB was supplied from Wakayama Seika Kogyo Co., Ltd. (Wakayama, Japan). The diamines, HAB and APAF, were kept under vacuum at 40 °C before synthesis. N-Methyl-2-pyrrolidone (NMP), cyclohexane, and o-xylene were purchased from Sigma-Aldrich Co. LLC (St. Louis, MO).

2.2. Synthesis of precursor hydroxyl polyimides

HPIs were synthesized from the 6FDA dianhydride and the two different diamines, APAF and HAB, using a two-step synthesis of polycondensation and solution-imidization [62]. Homopolymers were labeled as APAF-6FDA and HAB-6FDA. APAF-6FDA and HAB-6FDA were synthesized using 6FDA with equimolar *o*-hydroxyl diamines of APAF or HAB. In detail, 50 mmol of diamine (10.812 g of HAB or 18.313 g of APAF) was dissolved in 50 mL of NMP in a nitrogen atmosphere. After the diamine was fully dissolved, the flask was cooled in an ice bath and 50 mmol of 6FDA (22.212 g) was added with an additional 50 mL of NMP. Then, the system was vigorously mixed using a mechanical stirrer for 20 h to form a homogeneous hydroxy poly(amic acid) (HPAA) solution. After the flask was connected to a Dean-Stark trap and a water-circulated condenser, 100 mL of *o*-xylene was added into the mixture as an azeotrope agent. Afterward, the mixture was mechanically stirred for 8 h at 190 °C to prepare precursor polyimides through solution-imidization. The condensed water and *o*-xylene were removed by distillation and the system temperature was cooled to below 100 °C. The hydroxypolyimide (HPI) solution was poured and precipitated into an ethanol/water mixture (v/v = 1:3) to obtain a fibrous polymer. After precipitation, the obtained polymer powder was filtered and washed several times with an ethanol/water mixture to remove residual solvent, and then was thoroughly dried at 180 °C for 12 h in a vacuum oven.

Hydroxyl co-polyimides (Co-HPIs) were synthesized from 6FDA and different molar ratios of APAF and HAB using the same synthetic routes used with the homopolymers. Co-HPIs prepared from the two different diamines are referred to as AH followed by the suffix -x and -y, in which the suffix represents the molar ratios of APAF and HAB, respectively. Co-HPIs are abbreviated by the prefix “Co-” and polymer blends are referred to with the prefix “Blend-”. For example, Co-AH55 and Blend-AH55 refer to a copolyimide and a polyimide blend, respectively, obtained with 50/50 mol%/mol% of APAF/HAB-6FDA in the total polyimide.

2.3. Membrane preparation

2.3.1. HPIs and Co-HPIs

HPIs and Co-HPIs were dissolved in NMP to prepare 15 wt% casting solutions, which were filtered with a 1.0 μm PTFE syringe filter. The filtrated solutions were cast on a clean, flat glass plate. The glass plates were put in a leveled vacuum oven at 80 °C overnight. Then, the casting plates were heated to 100 °C for 1 h, and then 150, 200, and 250 °C for 1.5 h each under vacuum to remove the casting solvent. Afterward, the glass plates were immersed in boiling deionized water and the membranes were peeled off from the glass plate. The obtained ductile and transparent polyimide films (10 x 25 cm) were dried at 120 °C under vacuum overnight.

2.3.2. HPI blends

APAF-6FDA and HAB-6FDA homopolymer powders were dissolved together in NMP at a specific molar ratio. The blending solutions were stirred for at least 24 hours until they became clear and all the polymers were completely dissolved. The 15 wt% casting solutions were filtered with a 1.0 μm PTFE syringe filter before casting. For example, to fabricate Blend-AH19 membranes, 10 mol% of APAF-6FDA homopolymer and 90 mol% of HAB-6FDA homopolymer were mixed. Then, the same fabrication procedure used for the HPI membranes was employed to make the HPI blend membranes.

2.3.3. Thermally rearranged (TR) polymers

HPI, Co-HPI, and HPI blend membranes were converted into TR-PBO membranes by heat treatment in an electric tube furnace (CSC 12/9/450H, Lenton, UK) with a maximum operating temperature and power of 1200 °C. The tube furnace was purged with argon gas at 300 sccm during thermal treatment to maintain inert conditions and the polymer precursor samples (10 x 15 cm sized films) were sandwiched between the ceramic plates. Additionally, a five-layered crystal baffle was placed at the ends of the tube furnace to pre-heat the flowing gas. The polyimides were heated with stepwise protocols in which the samples were initially heated to 300 °C at 5 °C min^{-1} and held at 300 °C for 1 h for the complete imidization and then heated again at 5 °C min^{-1} to the final thermal rearrangement temperature of 450 °C and maintained for 1 h. Finally, the heated samples were naturally cooled to room temperature with an average cooling rate of approximately -2 °C min^{-1}. The final membrane films showed 40-60 μm of thickness (Figure A1). The obtained TR-PBO membranes were coded with the prefix “TR-”. For example, the TR-PBO membrane prepared from Co-AH55 was named TR-Co-AH55.

2.4. Characterization

The chemical structures were observed by Fourier-transform infrared spectroscopy (FT-IR) with an attenuated total reflection (ATR) accessory (IlluminatIR, SensIR Technologies, Danbury, CT, USA). The inherent viscosity of the polyimides was determined using a Schott Viscometry System (AVS 370, Schott Instruments GmbH, Germany) combined with an Ubbelohde viscometer (SI Analytics, Type 530 13: Capillary No. Ic, K = 0.03) with an automatic piston burette (TITRONIC Universal) at 25 ℃. The polyimides were dissolved in dimethyl sulfoxide (DMSO) and 25 mg mL^{-1} of the polymer solution was used to measure the viscosity [63,64]. The prepared polyimide solution was diluted to five concentrations (4.0, 3.0, 2.0, 1.5, and 1.0 mg mL^{-1}), and the system automatically and repetitively recorded the efflux time five times. The reduced (η_{red}), and inherent (η) viscosity were calculated from the following equations.

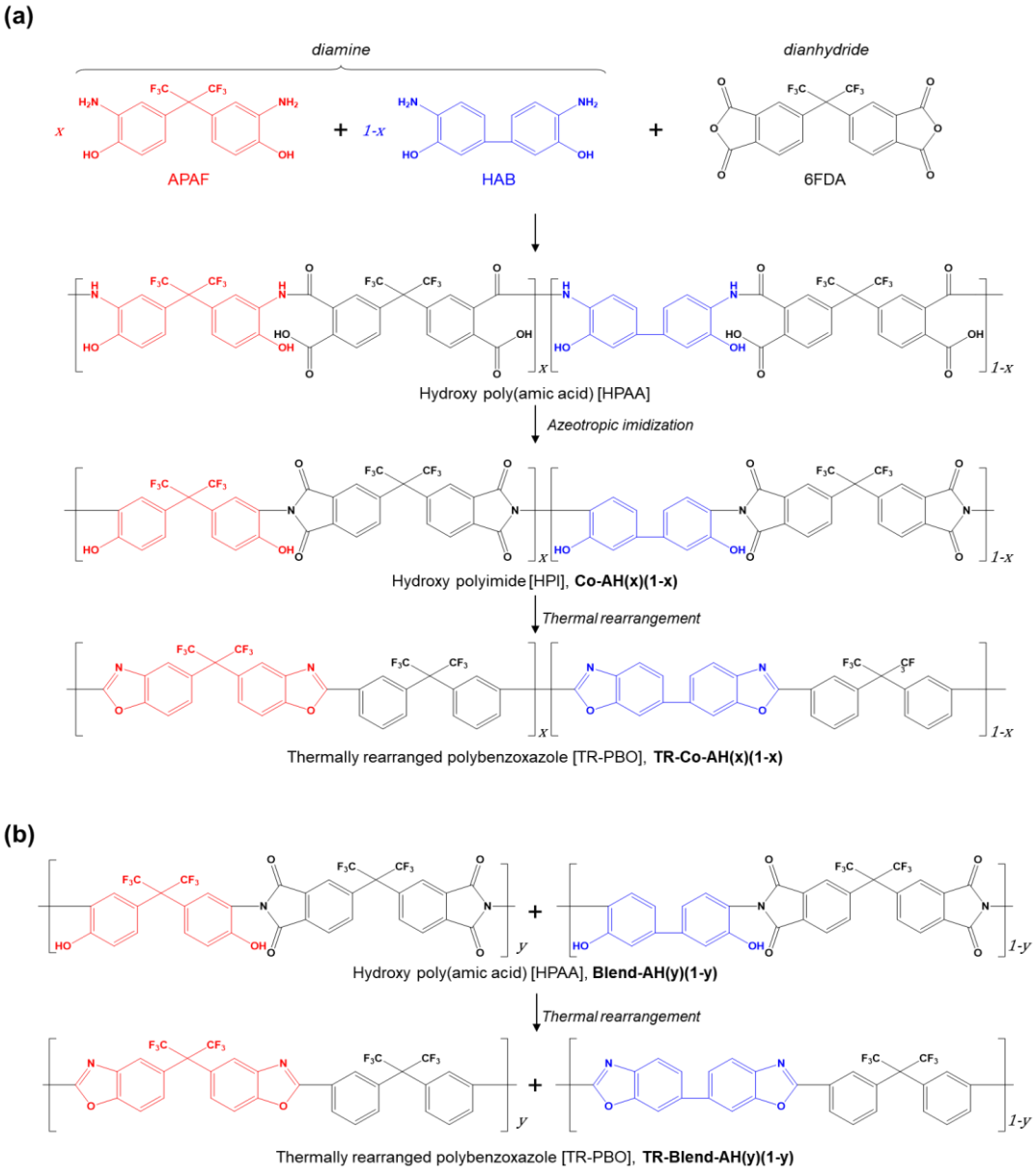

Scheme 1. Synthesis of (a) TR homo/copolymers and (b) TR polyblends with tailored APAF/HAB ratios, where *x* and *y* indicate the molar ratio of APAF over diamines for copolymers and polymer blends, respectively. The APAF/HAB ratios were controlled to be 0, 0.1, 0.3, 0.5, 0.7, 0.9, and 1 in this study. The bold words are sample codes for the corresponding polymers.

$$\eta_{red} = (\frac{t_1}{t_0} - 1)/c \quad (1)$$

$$\eta = (ln\frac{t_1}{t_0})/c \quad (2)$$

where t_0 and t_1 denote the efflux time of pure solvent and polymer solution, respectively, and c implies the concentration of the corresponding polymer solution.

The thermal properties of the membranes were measured with thermogravimetric analysis (TGA Q500, TA Instruments, DE, USA) up to 800 °C with a heating rate of 5 °C min^{-1} under nitrogen purging at a flow rate of 90 mL min^{-1}. Dynamic mechanical analysis (DMA Q800, TA Instruments, DE, USA) was used to measure the glass transition temperatures (T_g) of the polyimide membrane samples with a heating rate of 5 °C min^{-1} under a nitrogen atmosphere.

Microstructures of membrane films were visualized by field emission scanning electron microscopy (FE-SEM, Hitachi S-4800, Tokyo, Japan). The fractional free volumes (*FFVs*) of the TR membranes were calculated with the membrane density (ρ, g cm^{-3}) and van der Waals specific volume of the polymers (V_w, cm^3 g^{-1}), according to the following equation below [42],

$$FFV = 1 - 1.3\rho V_w \quad (3)$$

The ρ values of the membranes were obtained from a density measurement system (Sartorius LA 120 S, Sartorius AG, Gottingen, Germany), and V_w was evaluated using the MarvinSketch program (ChemAxon) [54].

Wide-angle X-ray diffraction (WAXD) measurements were carried out with a diffractometer (Rigaku Denki D/MAX-2500, Tokyo, Japan) with CuKα X-ray radiation (wavelength, λ = 0.154 nm) to investigate the interchain distance or *d*-spacing *(d)* of the membranes. The *d*-spacing value was calculated from the peak of the diffraction angle *(θ)* in the WAXD patterns based on Bragg's equation:

$$n\lambda = 2d\sin\theta \quad (4)$$

2.5. Gas permeation tests

A lab-made gas permeation system referred to as a time-lag apparatus was employed to measure the pure gas transport properties of the polymer membranes. For the time-lag measurement, testing cells, which membranes were sandwiched between aluminum foils, were used with an effective membrane area of 3.14 cm^2. Gas permeability was evaluated by a constant-volume/variable-pressure method at 35 °C under an upstream pressure of 1 bar for six gases (He, H_2, O_2, N_2, CO_2, and CH_4) by measuring the rate of pressure increase downstream under steady-state with

$$P = 10^{10} \times \frac{T_0 V_1 l}{A T p_2}\left(\frac{dp_1}{dt}\right) \quad (5)$$

where P (Barrer) is the gas permeability (1 Barrer = 10^{-10} cm^3 (STP)·cm·cm^{-2}·s^{-1}·$cmHg^{-1}$), T_0 (K) is the standard temperature, V_1 (cm^3) is the downstream volume, l (cm) is the membrane thickness, T (K) is the measurement temperature, p_2 (cmHg) is the upstream pressure, A (cm^2) is the effective membrane area, and dp_1/dt (cmHg·s^{-1}) is the rate of pressure increase downstream. The ideal gas selectivity (α) was obtained from the permeability ratio between two gases with

$$\alpha = \frac{P_i}{P_j} \quad (6)$$

where the subscripts i and j indicate faster and slower gas species, respectively.

The diffusivity *(D)* was obtained from the time-lag (θ, sec) and membrane thickness (l, cm) following the equation below.

$$D = \frac{l^2}{6\theta} \quad (7)$$

The solubility was calculated by dividing gas permeability *(P)* with diffusivity *(D)* based on the solution-diffusion transport model equation.

$$S = \frac{P}{D} \quad (8)$$

3. Results and discussion

3.1. HPI synthesis and thermal rearrangement

HPI homopolymers and copolymers were successfully synthesized as depicted in Scheme 1 and obtained with enough inherent viscosity for membrane casting [57] as shown in Table A1. Their chemical structures were confirmed by ATR FT-IR after casting the copolymer or polymer blend membranes. All FT-IR spectra of the HPIs showed clear imide functional peaks at 1790 and 1715 cm^{-1} from the C=O double bonds and at 1382 cm^{-1} from the C–N bond of imide rings. Also, a broad absorbance peak appeared at ~3200 cm^{-1}, indicating -OH groups in the HPIs (Figure 1a). After TR conversion, the -OH and imide peaks disappeared while peaks at 1480 and 1054 cm^{-1} were observed, indicating C-N and C-O-C bonds in the benzoxazole group, respectively (Figure 1b). The carbonyl peaks at ~1700 cm^{-1} partially remained from the unreacted imide residues; however, other imide peaks at 1790 cm^{-1} and 1382 cm^{-1} disappeared after the conversion. Therefore, it could be said that most hydroxyl imides were converted into benzoxazoles after the TR process.

3.2. Thermal properties

The thermal properties of the HPI precursors were characterized by TGA and DMA to confirm thermal stability and determine TR conversion. The thermomechanical properties are summarized in Table A2. The TGA graphs of the HPIs showed a two-step weight loss with increasing temperature up to 800 °C, where the first and second weight losses were separately observed at temperature ranges of 350–450 °C and above 500 °C, respectively (Figure 2). As two equivalent CO_2 molecules were discharged during the TR reaction, the first weight loss was induced from the imide-benzoxazole conversion, whereas the second one was from the thermal degradation of the TR polymers. The homopolymers of HAB-6FDA and APAF-6FDA showed 14.50 and 11.18% weight loss during TR conversion, respectively, which agreed very well with the corresponding theoretical value. Here, the theoretical value of TR conversion was calculated by changes in molecular weight of a repeating unit between HPI precursors and TR-PBOs. Likewise, copolyimides and polyimide blends showed reasonable weight losses close to their theoretical values (Figure A2). Their weight losses during TR conversion increased with the APAF fraction due to the larger weight loss in APAF-6FDA than in the HAB-6FDA precursors. These results showed that the copolyimides exhibited very similar weight loss to the corresponding polyimide blends that contained the same APAF/HAB ratio in the total polymer. For example, Co-AH55 and Blend-AH55 had 12.75 and 12.36% TR weight losses, respectively, and both values were close to their theoretical values of 12.58%. Therefore, TR conversion was not disturbed in the multicomponent polymer systems, regardless of the binding types.

For an in-depth understanding of the changes in chain mobility during the TR process, the thermomechanical properties of the HPIs were monitored with increasing temperature. The homopolymers showed typical DMA curves of the TR precursors in which the storage modulus initially maintained a plateau but then sharply dropped and was restored with heating (Figure 3) [65]. The glass transition temperature (T_g), which was obtained from the maximum Tan δ peak, was 321 and 413 °C for APAF-6FDA and HAB-6FDA, respectively. APAF-6FDA exhibited a much lower T_g than HAB-6FDA because the bulky hexafluoroisopropylidene groups in APAF effectively hindered chain packing and endowed the polymer chains with higher flexibility. Due to the chain rigidity of the precursor HPIs, HAB-6FDA showed a higher onset temperature of TR conversion where the storage modulus started to be recovered than APAF-6FDA because the solid-state reaction occurred when the precursor polymer chain had enough mobility to be rearranged.

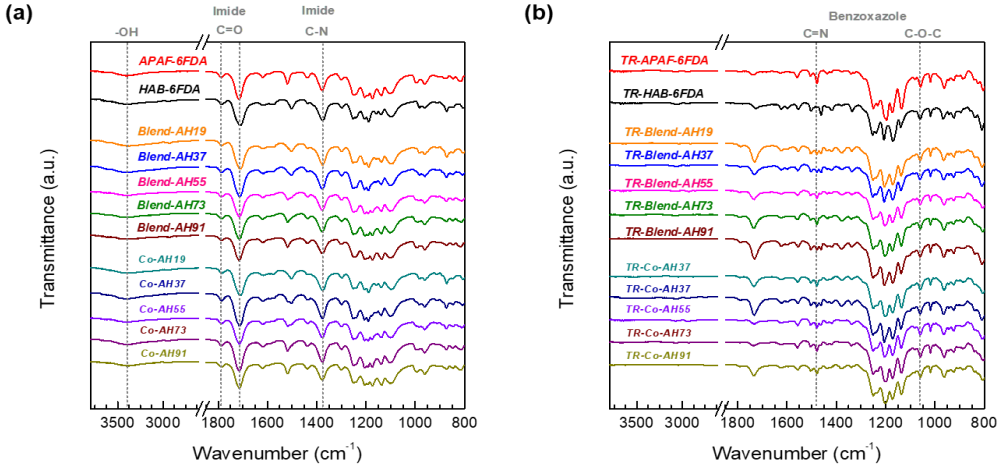

Fig. 1. ATR FT-IR spectra for (a) hydroxy polyimides and (b) TR polybenzoxazoles. Each spectrum corresponds with the sample code in the same color in the graph.

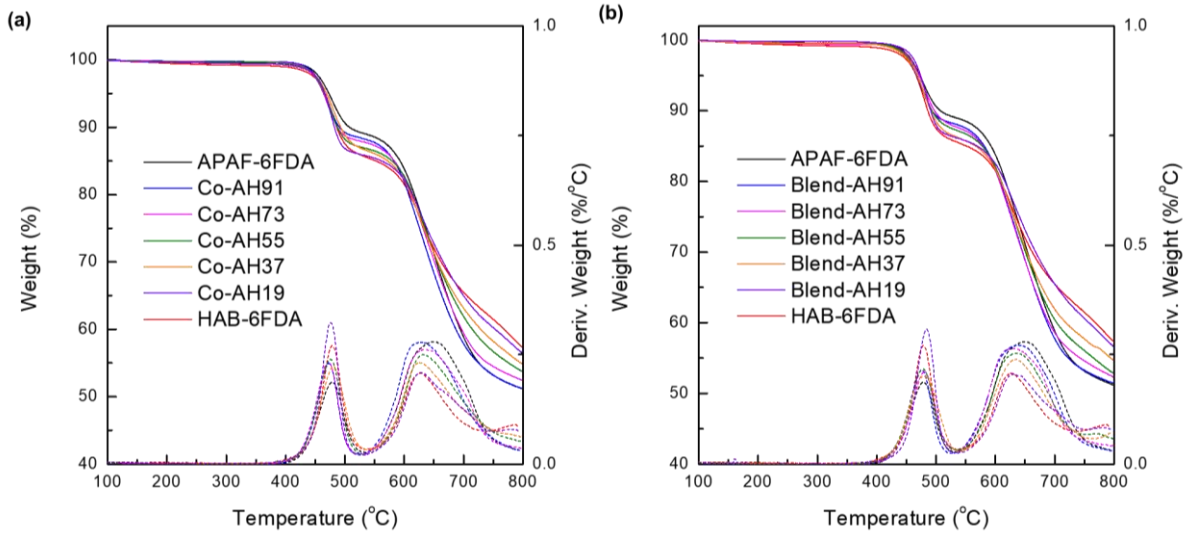

Fig. 2. TGA graphs of (a) copolyimides and (b) polyimide blends with various APAF fractions. The values of solid and dashed lines correspond to the left (Weight) and right (Deriv. Weight) Y-axes, respectively.

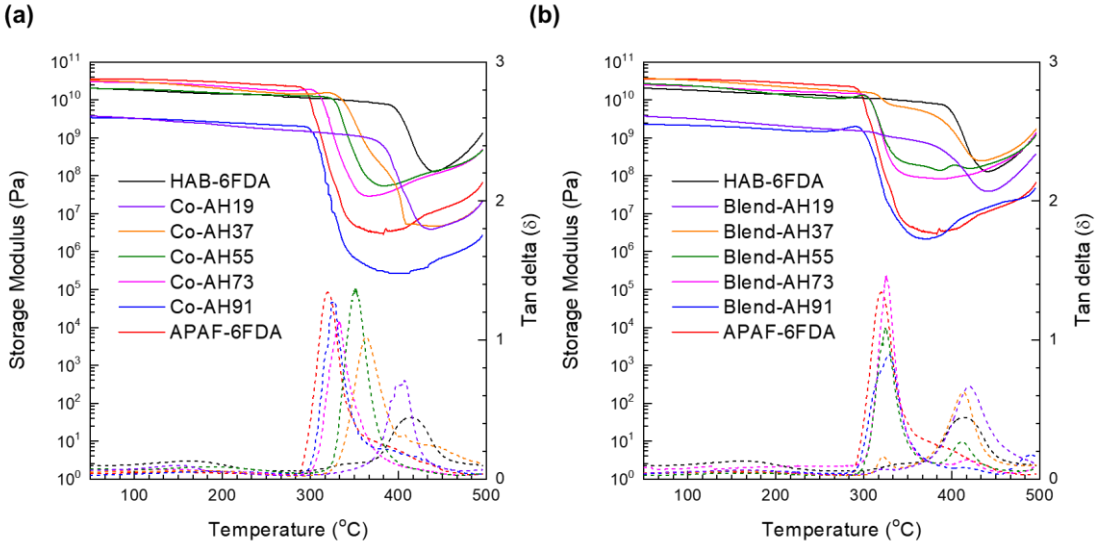

Fig. 3. DMA curves of **(a)** copolyimides and **(b)** polyimide blends with various APAF fractions. The values of the solid and dashed lines correspond to the left (Storage modulus) and right (tan δ) Y-axis, respectively.

The copolyimides displayed the same behavior of thermomechanical properties as the homopolymers with a single Tan δ peak. The T_gs of the copolyimides were always between that of APAF-6FDA and HAB-6FDA and increased with the amount of the HAB moiety, following the Fox equation (Figure A3) [66]. For example, Co-AH55 had a T_g at 352 °C that was close to the calculated value of 361 °C from the Fox equation. On the contrary, the polyimide blends exhibited two distinctive Tan δ peaks and each peak temperature was close to the T_g of each homopolymer component, APAF-6FDA, and HAB-6FDA. Moreover, the intensities of the Tan δ peaks were proportional to the weight fraction of each homopolymer in the polyimide blends. This phenomenon was attributed to the fact that the two physically mingled polymer chains in the polyblends independently influenced their thermomechanical behaviors.

3.3. Physical properties

All polymer solutions, including homopolymers, copolymers, and polymer blends, were cast as clear and transparent films. As shown in SEM images (Figure A1), all the membranes exhibited miscible, homogenous, and continuously dense phases without noticeable defects or phase separations.

XRD analysis with the *d*-spacing calculation based on Bragg's equation confirmed the microporosity and interchain distances of the polymer membranes (Table A3). All the samples exhibited the amorphous character of polymers, displaying a broad halo in the XRD profile of 2θ between 10 and 20° (Figure 4). After TR conversion, the XRD peaks of all precursor polyimides were shifted toward smaller 2θ regions as guided by the horizontal black dashed lines in the graphs, indicating enlargement of the *d*-spacing. In fact, the XRD peaks of the precursors were at 2θ of 15.05–16.32°, which corresponded to a *d*-spacing of 0.54–0.59 nm, while those of TR polymers moved toward *d*-spacings of 0.61–0.68 nm. For example, the *d*-spacing increased from 0.56 to 0.62 nm for APAF-6FDA after TR conversion, and for Co-AH55 and Blend-AH55, the *d*-spacing was enhanced from 0.59 and 0.57 nm, respectively, to 0.62 nm. Therefore, an increment of interchain distance during TR conversion was observed in all types of precursor polyimides.

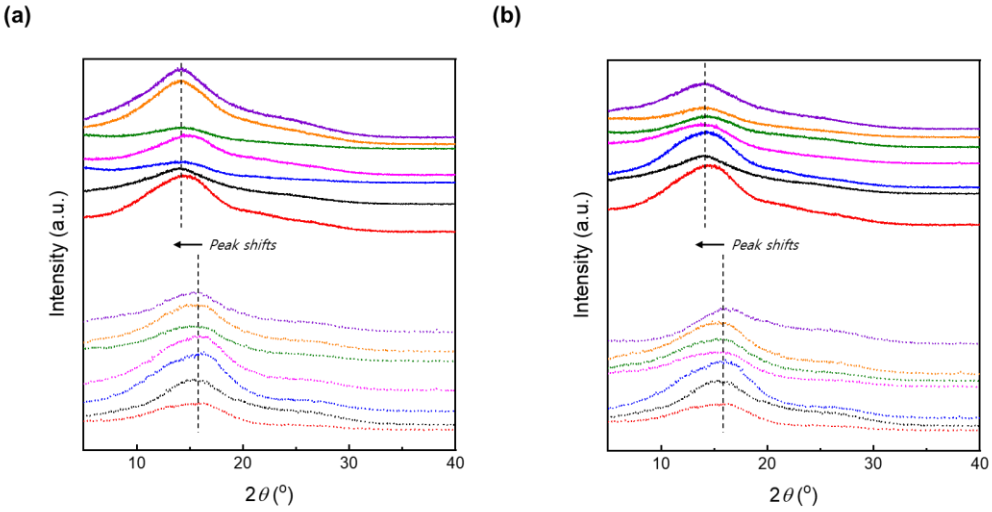

Fig. 4. XRD profiles of the membranes from **(a)** copolymerization and **(b)** polymer blending. The solid and dashed lines in the graphs represent TR polymers and polyimides, respectively. The line colors indicate each polymer, APAF-6FDA (red), HAB-6FDA (black), AH91 (blue), AH73 (magenta), AH55 (olive), AH37 (orange), and AH19 (violet). The black horizontal dashed lines across the XRD profiles indicate the average scattering vectors (2θ) of each polymer group.

Table 1
Physical properties of TR polymers.

Code	V_w (cm^3 g^{-1})	ρ (g cm^{-3})	*FFV*
TR-HAB-6FDA	0.468	1.364	0.170
TR-Co-AH19	0.464	1.367	0.175
TR-Co-AH37	0.457	1.385	0.177
TR-Co-AH55	0.451	1.398	0.181
TR-Co-AH73	0.445	1.415	0.181
TR-Co-AH91	0.440	1.432	0.181
TR-Blend-AH19	0.464	1.364	0.177
TR-Blend-AH37	0.457	1.382	0.179
TR-Blend-AH55	0.451	1.393	0.184
TR-Blend-AH73	0.445	1.409	0.185
TR-Blend-AH91	0.440	1.421	0.187
TR-APAF-6FDA	0.437	1.433	0.186

V_W – Specific Van der Waals Volume, ρ – membrane density, *FFV* – fractional free volume.

The microporosity of the TR polymers was further investigated by *FFV* measurements. As listed in Table 1, all the resultant TR polymers had *FFV*s of 17.0–18.7%, depending on their chemical structures and casting methods. For the two TR homopolymers, TR-APAF-6FDA possessed 1.6% more *FFV* compared to TR-HAB-6FDA because the bulky fluorinated units in APAF provided additional free volume elements in the TR matrix. Moreover, the *FFV*s of the TR copolymers and the TR polyblends gradually increased with the APAF fraction. For example, the TR polymers with an APAF fraction of 0.9 (TR-Co-AH91 and TR-Blend-AH91) showed 0.6 and 1.0% more *FFV*s than their counterparts containing an APAF fraction of 0.1 (TR-Co-AH19 and TR-Blend-AH19), respectively. Interestingly, the TR-Blend-AHs always showed higher *FFV*s than the corresponding TR-Co-AHs, which were prepared from the same APAF/HAB ratio. For example, the *FFV* of TR-Blend-AH55 was 18.4% while that of TR-Co-AH55 was 18.1%. This indicated that TR conversion was more effective for microporosity formation on the physically mixed chain configuration of polyimide blends than on chemically bonded copolyimides. Additionally, TR-Blend-AH91, which contained the highest APAF fraction among the TR blend samples, showed a slightly higher *FFV* than TR-APAF-6FDA (18.7 vs. 18.6%).

3.4. Gas transport behavior

The pure gas permeability and selectivity of the precursor HPIs and TR polymers were measured for the six representative small gases, He, H_2, CO_2, O_2, N_2, and CH_4, at 35 °C at 1 bar, and the results are listed in Table 2. The gas permeability of all the membranes mostly followed the order of the kinetic diameters of the gas molecules, suggesting typical diffusion-selective glassy polymer properties. Among the precursor polyimides, there was no considerable difference in gas transport properties regardless of the casting methods or compositions due to the similar gas permeability of the two homopolyimides. In fact, the CO_2 permeability of HAB-6FDA and APAF-6FDA was 9.5 and 11 Barrer, respectively. After TR conversion, a significant enhancement in gas permeability was observed for all precursors, and moreover, TR-APAF-6FDA showed a much higher gas permeability ($P(CO_2)$ = 510 Barrer) than TR-HAB-6FDA ($P(CO_2)$ = 270 Barrer), corresponding well with their *FFV*s and our previous reports [35,67]. Because the APAF units contained a bulky fluorinated segment (CF_3-C-CF_3) and effectively reduced the chain rigidity of the precursor polyimide, additional free volume formation via chain rearrangement during TR conversion was much more remarkable in APAF-6FDA, resulting in higher gas permeability. Consequently, both TR copolymers and polyblends showed gradually increasing gas permeability with increasing APAF moieties. For example, TR-Co-AH19 and TR-Blend-AH-19 exhibited CO_2 permeability values of 243 and 288 Barrer whereas that of TR-Co-AH91 and TR-Blend-AH-91 was 495 and 603 Barrer, respectively. Thus, the fluorinated content improved the gas transport of TR polymers derived from not only homopolymers but also copolymers and polymer blends. Furthermore, diffusivities and solubilities of CO_2 and CH_4 were obtained from time-lags of the resulting TR polymers, as listed in Table A4. The same trends with gas permeability were observed in gas diffusion and sorption, where both diffusivity and solubility increased with increasing bulky perfluoro moieties.

Comparing the TR polymers from the copolyimides and the polyimide blends, the TR polyblends always showed a higher gas permeability and comparable gas selectivity relative to their counterpart TR copolymers that contained the same APAF/HAB ratio (Figure 5). For example, the CO_2 permeability of TR-Co-AH73 was 386 Barrer whereas TR-Blend-AH73 had a 25% higher permeability of 484 Barrer. As discussed above, each multicomponent polymer had distinct thermomechanical properties and showed different chain mobility, which influenced the microporous structures constructed during the TR process. Hence, although the TR polymers were prepared from the same monomers with the same thermal treatments, they present distinguishable gas transport behaviors, which were often observed in polymer membranes [68-70].

Table 2
Gas permeability and ideal gas selectivity of HPIs and TR polymers measured at 35 °C and 1 bar. Gas permeation is the average value from at least two specimens with less than 10% error.

Code	Permeability (Barrer)						Ideal selectivity					
	He	H_2	O_2	N_2	CH_4	CO_2	H_2/N_2	CO_2/N_2	O_2/N_2	H_2/CH_4	CO_2/CH_4	N_2/CH_4
HAB-6FDA	45	34	2.1	0.37	0.13	9.4	92	25	5.7	268	73	2.9
Blend-AH19	52	39	2.7	0.39	0.14	10	100	27	7.1	275	73	2.8
Blend-AH37	57	41	2.9	0.42	0.15	11	98	26	6.9	282	75	2.9
Blend-AH55	58	39	2.8	0.59	0.11	9.4	66	16	4.7	351	84	5.3
Blend-AH73	61	39	2.7	0.38	0.11	9.3	103	25	7.1	356	85	3.5
Blend-AH91	64	40	2.9	0.42	0.12	10	97	24	7	344	83	4
Co-AH19	50	36	2.7	0.37	0.14	8.4	97	23	7.3	255	60	2.6
Co-AH37	57	39	2.4	0.35	0.11	9.4	110	27	6.7	344	83	3.1
Co-AH55	65	44	3	0.53	0.23	11	82	20	5.6	191	48	2.3
Co-AH73	61	39	2.5	0.43	0.16	9.4	91	22	5.7	247	59	2.7
Co-AH91	64	40	2.9	0.53	0.18	10	76	19	5.4	220	55	2.9
APAF-6FDA	75	46	2.9	0.48	0.15	11	94	22	6.1	307	72	3.3
TR-HAB-6FDA	236	312	55	13	12	270	24	21	4.2	26	23	1.1
TR-Blend-AH19	251	326	56	14	11	288	24	21	4.2	30	26	1.2
TR-Blend-AH37	309	404	73	18	14	364	23	21	4.2	29	26	1.3
TR-Blend-AH55	381	488	100	26	20	477	19	18	3.9	24	23	1.3
TR-Blend-AH73	406	529	107	28	22	484	19	17	3.8	24	22	1.3
TR-Blend-AH91	506	621	127	34	24	603	18	18	3.7	25	25	1.4
TR-Co-AH19	232	292	51	12	11	243	24	20	4.3	27	22	1.1
TR-Co-AH37	279	356	65	16	13	325	23	21	4.1	28	26	1.3
TR-Co-AH55	302	358	61	15	10	290	25	20	4.2	35	28	1.4
TR-Co-AH73	388	452	85	21	17	386	21	18	4	27	23	1.2
TR-Co-AH91	424	510	112	29	21	495	18	17	3.9	24	24	1.4
TR-APAF-6FDA	488	581	116	31	22	510	19	16	3.7	27	23	1.4

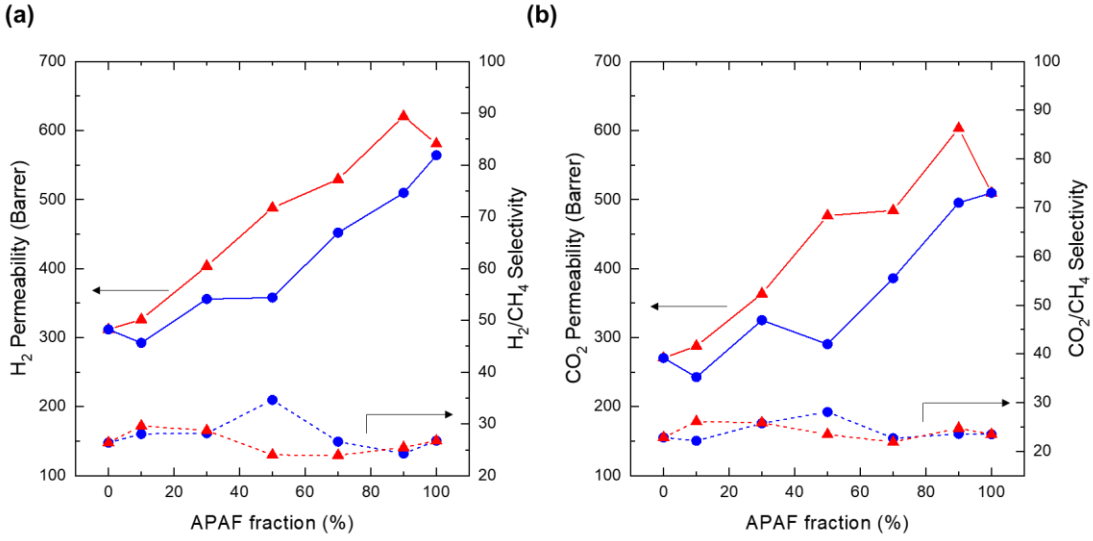

Fig. 5. Gas permeability and selectivity of TR polymers as a function of APAF fraction for **(a)** H_2/CH_4 and **(b)** CO_2/CH_4 gas pairs. Blue circles and red triangles indicate TR copolymers and TR polyblends, respectively. Gas permeation is the average value from at least two specimens with less than 10% error.

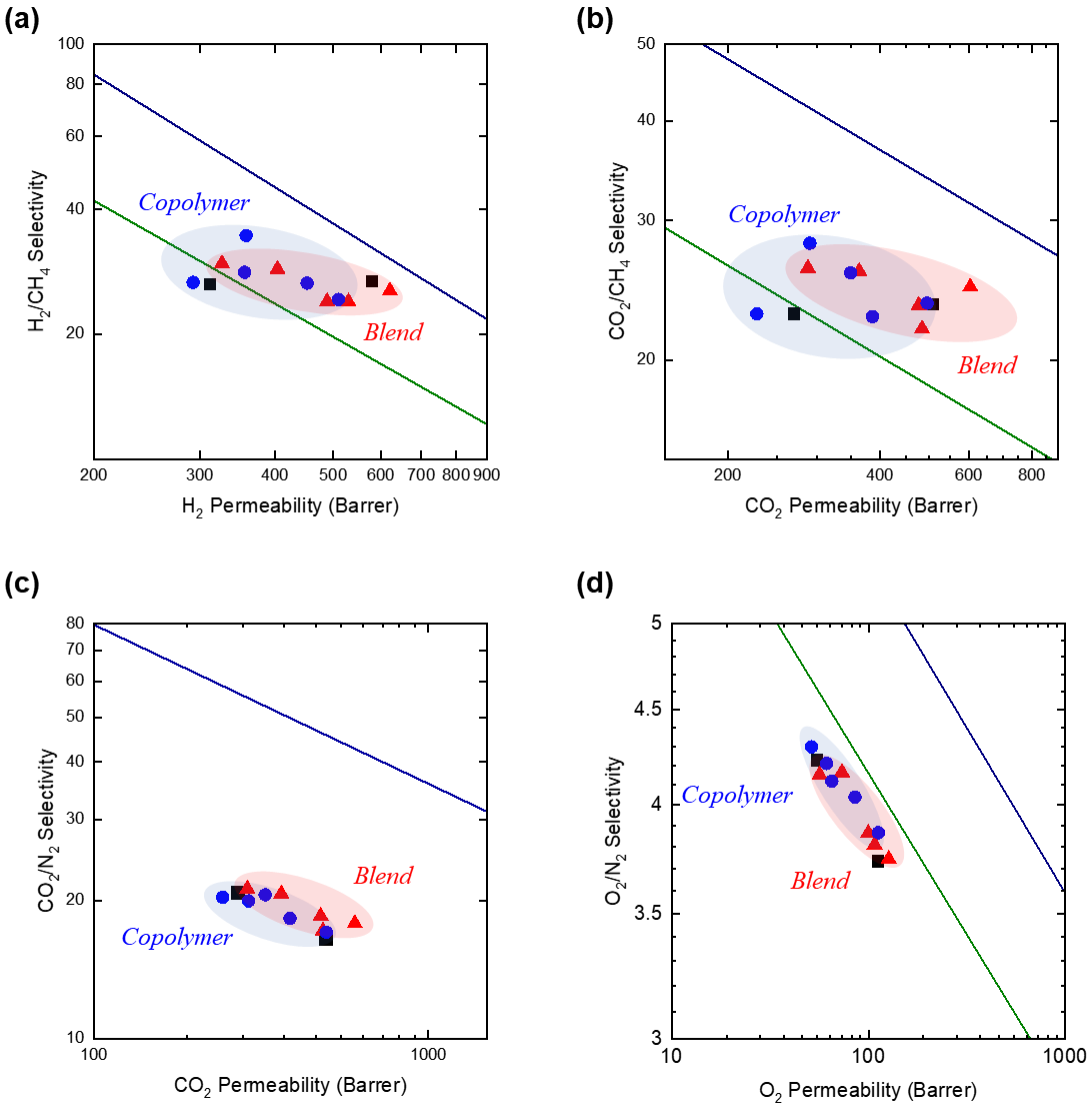

Fig. 6. Robeson upper bound plots for (a) H_2/CH_4, (b) CO_2/CH_4, (c) CO_2/N_2, and (d) O_2/N_2. TR polymers are presented in the plots [TR homopolymers (TR-APAF-6FDA and TR-HAP-6FDA, black rectangles), TR-Co-AHs (blue circles), and TR-Blend-AHs (red triangles)]. Olive and blue solid lines indicate 1991 and 2008 upper bounds [8,71].

The gas separation performance of the TR homopolymers, copolymers, and polymer blends was illustrated in Robeson upper bound plots for hydrogen recovery (H_2/CH_4), carbon captures (CO_2/N_2 and CO_2/CH_4), and air separation (O_2/N_2) (Figure 6). As discussed above, the TR blends are located at the higher permeability region compared with the corresponding TR copolymers. Overall, the gas permeability of the resultant TR copolymers and polyblends were located between TR-HAB-6FDA and TR-APAF-6FDA, depending on the APAF fraction except for TR-Co-AH19 and TR-Blend-AH91. The gas permeabilities of TR-Co-AH19 were lower than those of TR-HAB-6FDA. For example, the CO_2 permeability of the copolymer was only 243 Barrer. In contrast, the gas permeability of TR-Blend-AH91 exceeded that of TR-APAF-6FDA, for example, having a high CO_2 permeability of 603 Barrer. We assumed that the higher gas permeability of TR blends than that of TR copolymers in the same composition was from the localized phases of each component [59,60,68]. The microstructures of the TR blends in the mixed matrices were definitely different from the TR copolymer counterparts, which phase is ultimately homogeneous. The formation of the microporous structures of the TR copolymers and the TR blends were highly influenced by the membrane preparation method and the interaction between each polymer's components as well as their chemical structures. Moreover, the TR polymers in this study were presented in Robeson plots with reported TRs with recently redefined upper bounds [72,73] to give an at-a-glance view of their overall gas separation performance (Figure A4).

4. Conclusions

Precursor HPI homopolymers and copolymers were successfully synthesized with sufficient inherent viscosity for membrane casting. After that, a series of TR polymers were prepared from thermal treatment on either copolyimide or polyimide blends that contained different APAF/HAB monomer ratios. The TR conversion of all HPIs was confirmed by ATR FT-IR, TGA, and DMA analysis. The HPI copolymers showed one T_g that agreed well with the Fox equation whereas the HPI polymer blends exhibited two distinguishable T_gs because the physically mixed homopolymer chains maintained their respective thermomechanical properties. Furthermore, the TR polymer blends had larger *FFV*s and therefore higher gas permeability than their counterpart TR copolymers that were prepared from the same composition of monomers. Also, the gas permeability increased with the APAF moiety in both the TR copolymers and polyblends due to the presence of bulky hexafluoroisopropylidene units in the polymers. As a conclusion, it was confirmed that the gas transport behaviors of the TR polymers could be tailorable by the contents of the fluorinated segments and by controlling the multicomponent polymer system.

Appendix

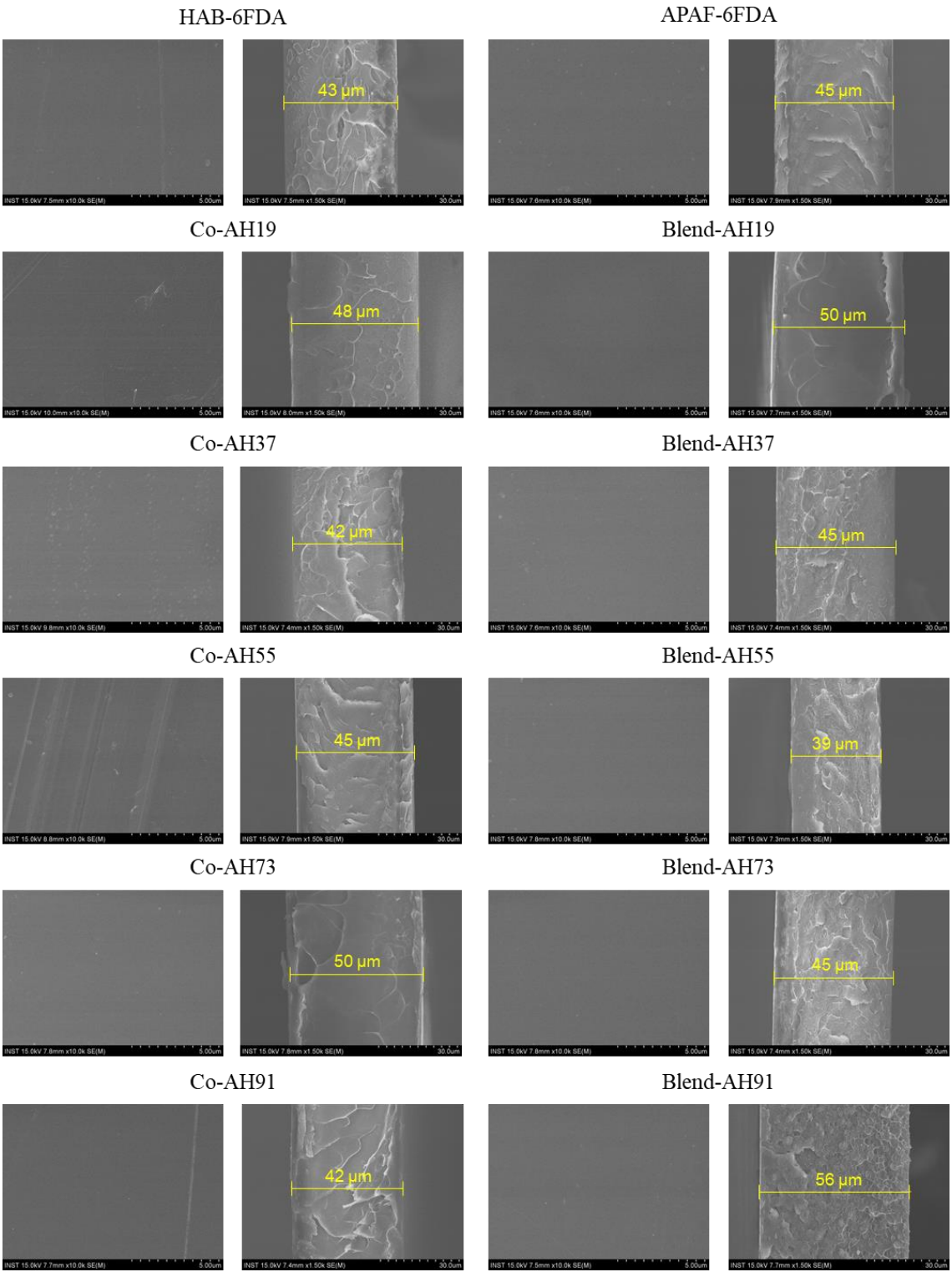

Fig. A1. SEM images of the membrane films at the surface (left images) and cross-section (right images) for each sample.

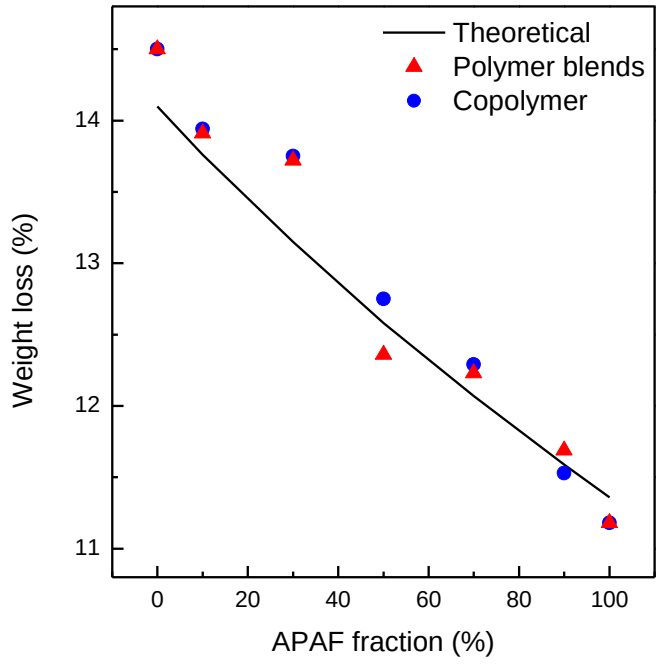

Fig. A2. Weight loss of HPI copolymers and polymer blends during TR conversion. The black solid line is the theoretical weight loss at the specific APAF fraction.

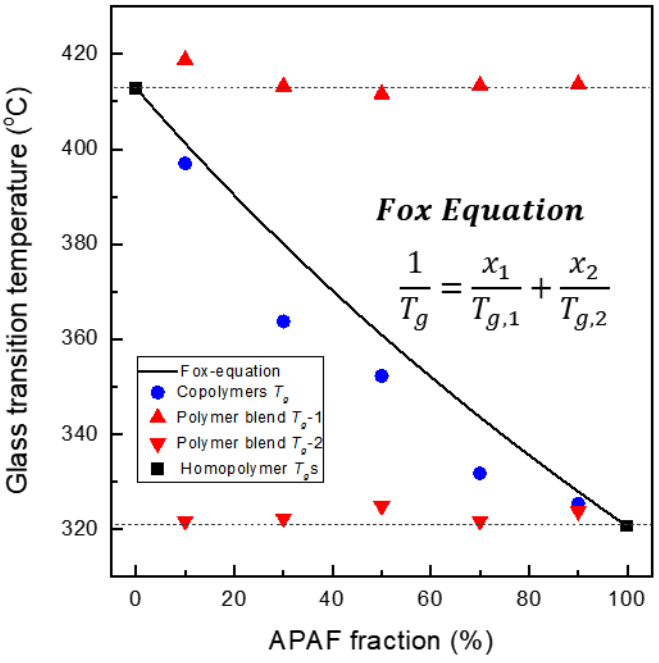

Fig. A3. Glass transition temperatures (T_g) of HPI homopolymers, copolymers, and polymer blends obtained from DMA. A solid line was drawn from the Fox equation, and the two dashed lines indicate the T_gs of APAF-6FDA (the lower) and HAB-6DFA (the upper), respectively.

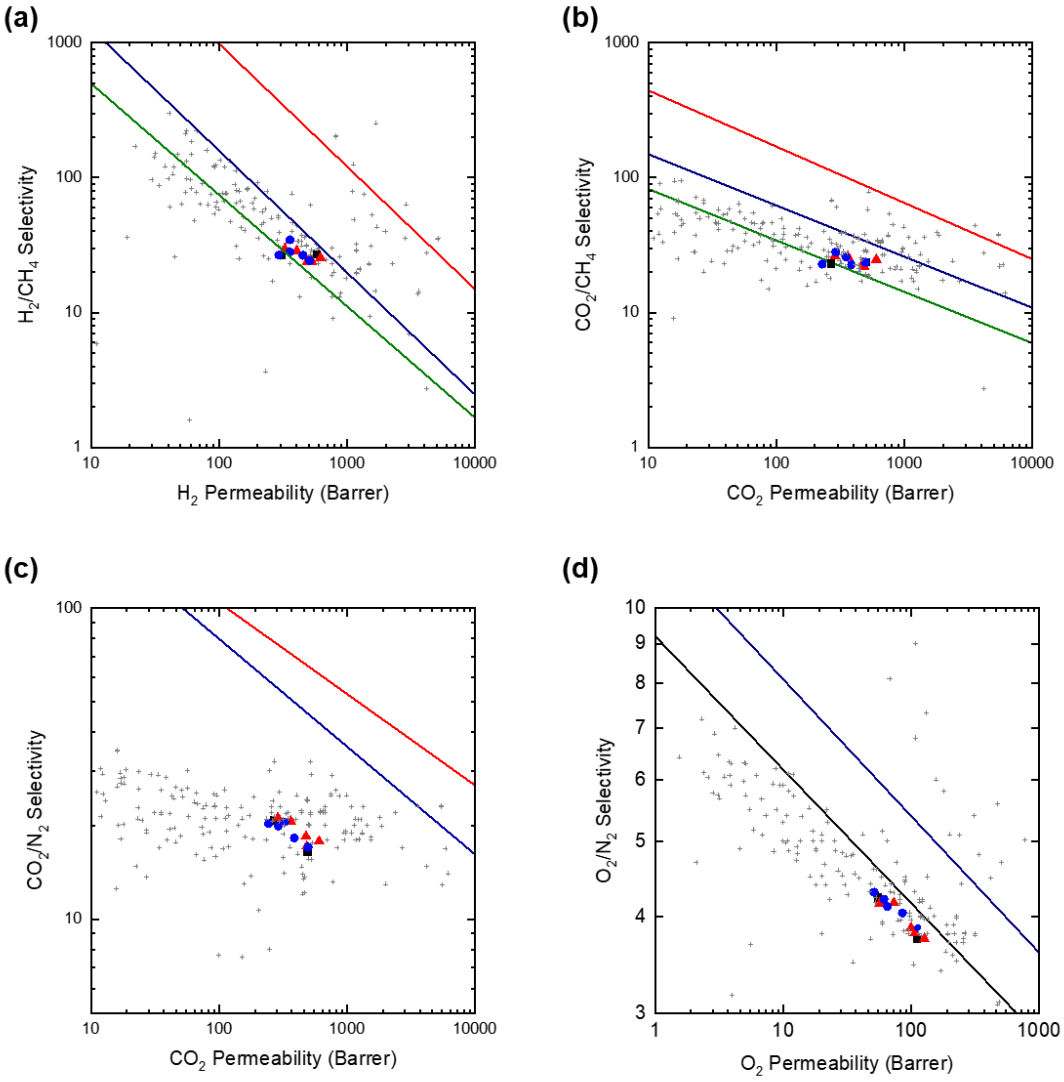

Fig. A4. Robeson upper bound plots for **(a)** H_2/CH_4, **(b)** CO_2/CH_4, **(c)** CO_2/N_2, and **(d)** O_2/N_2. TR homopolymers (TR-APAF-6FDA and TR-HAP-6FDA, black rectangles), TR-Co-AHs (blue circles), and TR-Blend-AHs (red triangles), and reported TR polymers (gray crosses) [16,74]. Solid lines in the graphs are upper bounds [8,72,73].

Table A1
Inherent viscosity of hydroxy polyimides.

Code	Inherent viscosity (dL/g)
HAB-6FDA	0.344
Co-AH19	0.790
Co-AH37	0.421
Co-AH55	0.466
Co-AH73	0.659
Co-AH91	1.441
Blend-AH19	0.327
Blend-AH37	0.372
Blend-AH55	0.521
Blend-AH73	0.520
Blend-AH91	0.382
APAF-6FDA	0.710

Table A2
Thermal properties of hydroxyl polyimides.

Code	Conversion temperature (°C)			Weight loss (%)		Char yield at 800 °C (%)
	T_g	T_{TR1}	T_{TR2}	Theo.	Exp.	
HAB-6FDA	413	329	430	11.36	14.40	57.49
Co-AH19	397	330	428	13.76	13.89	56.56
Co-AH37	364	331	433	13.15	13.52	54.97
Co-AH55	352	331	430	12.58	12.61	52.95
Co-AH73	332	326	425	12.07	12.05	52.46
Co-AH91	325	334	425	11.59	11.43	51.23
Blend-AH19	322/419	326	435	13.76	13.76	56.73
Blend-AH37	322/413	326	429	13.15	13.15	55.52
Blend-AH55	325/412	328	428	12.58	12.90	53.8
Blend-AH73	322/413	325	431	12.07	12.25	52.4
Blend-AH91	324/414	324	429	11.59	11.69	51.48
APAF-6FDA	321	332	431	14.10	11.05	51.26

T_g - Obtained from tan δ of DMA.
T_{TR1} – Obtained from TGA. The onset temperature of thermal rearrangement.
T_{TR2} – Obtained from TGA. The first peak of the derivation of the weight (% $°C^{-1}$) curve during thermal rearrangement.

Table A3
XRD peak properties of HPIs and TR polymers.

Code	HPI		TR	
	2θ (°)	*d*-spacing (nm)	2θ (°)	*d*-spacing (nm)
HAB-6FDA	15.91	0.56	14.36	0.62
Co-AH19	15.77	0.56	13.85	0.64
Co-AH37	15.13	0.59	13.87	0.64
Co-AH55	15.05	0.59	14.17	0.62
Co-AH73	15.93	0.56	14.46	0.61
Co-AH91	16.31	0.54	13.6	0.65
Blend-AH19	15.95	0.56	14.07	0.63
Blend-AH37	15.62	0.57	14.09	0.63
Blend-AH55	15.58	0.57	14.36	0.62
Blend-AH73	15.67	0.57	13.77	0.64
Blend-AH91	16.05	0.55	12.97	0.68
APAF-6FDA	15.48	0.57	14.17	0.62

Table A4
Diffusion and sorption of CO_2 and CH_4 for TR polymers.

Code	Diffusivity (10^{-9} cm^2/s)		Solubility [cm^3(STP)/cm^3 (polymer)·atm]		Diffusion selectivity	Solubility selectivity
	CO_2	CH_4	CO_2	CH_4	CO_2/CH_4	CO_2/CH_4
TR-HAB-6FDA	98	21	21	4.3	4.7	4.9
TR-Blend-AH19	105	18	21	4.6	5.8	4.5
TR-Blend-AH37	133	20	21	5.3	6.6	3.9
TR-Blend-AH55	171	28	21	5.5	6.0	3.9
TR-Blend-AH73	231	33	16	5.1	7.0	3.1
TR-Blend-AH91	237	42	19	4.4	5.6	4.4
TR-Co-AH19	94	18	20	4.6	5.1	4.3
TR-Co-AH37	110	16	23	5.8	6.7	3.9
TR-Co-AH55	121	19	18	4.2	6.4	4.4
TR-Co-AH73	166	26	18	4.9	6.3	3.6
TR-Co-AH91	185	34	20	4.7	5.4	4.4
TR-APAF-6FDA	191	35	20	4.7	5.4	4.4

Acknowledgments

This research was supported by the Technology Development Program to Solve Climate Change administered through the National Research Foundation of Korea (NRF), funded by the Ministry of Science and ICT (NRF-2018M1A2A2061979). Additional funding came from a Korea Institute of Energy Technology Evaluation and Planning (KETEP) grant funded by the Ministry of Trade, Industry, and Energy of the Republic of Korea (MOTIE) (20202020800330).

References

[1] R.W. Baker, Future directions of membrane gas separation technology, Ind. Eng. Chem. Res. 41 (2002) 1393-1411. https://doi.org/10.1021/ie0108088

[2] Y. Labreche, Functionalized polymeric membranes for CO2 capture, J. Membr. Sci. Res., 2 (2016) 59-65. https://doi.org/10.22079/JMSR.2016.19153

[3] A. Sharif, Polymeric Gas Separation Membranes: What Makes them Industrially more Attractive?, J. Membr. Sci. Res., 4 (2018) 2-3. https://doi.org/10.22079/jmsr.2017.71695.1158

[4] Y. Zhuang, J.G. Seong, Y.M. Lee, Polyimides containing aliphatic/alicyclic segments in the main chains, Prog. Polym. Sci., 92 (2019) 35-88. https://doi.org/10.1016/j.progpolymsci.2019.01.004

[5] W.J. Koros, G. Fleming, Membrane-based gas separation, J. Membr. Sci., 83 (1993) 1-80. https://doi.org/10.22079/jmsr.2017.71695.1158

[6] H. Sanaeepur, R. Ahmadi, M. Sinaei, A. Kargari, Pebax-modified cellulose acetate membrane for CO2/N2 separation, J. Membr. Sci. Res., 5 (2019) 25-32. https://doi.org/10.22079/JMSR.2018.85813.1190

[7] X.Y. Chen, T.B. Nguyen, A. Romero, A. Patón, M. Sanchez, J. Valverde, S. Kaliaguine, D. Rodrigue, Gas separation properties of mixed matrix membranes based on polyimide and graphite oxide, J. Membr. Sci. Res., 6 (2020) 58-69. http://doi.org/10.22079/JMSR.2019.100069.1244

[8] L.M. Robeson, The upper bound revisited, J. Membr. Sci., 320 (2008) 390-400. https://doi.org/10.1016/j.memsci.2008.04.030

[9] X. Hu, W.H. Lee, J.Y. Bae, J. Zhao, J.S. Kim, Z. Wang, J. Yan, Y.M. Lee, Highly permeable polyimides incorporating Tröger's base (TB) units for gas separation membranes, J. Membr. Sci., 615 (2020) 118533. https://doi.org/10.1016/j.memsci.2020.118533

[10] X. Hu, W.H. Lee, J. Zhao, J.Y. Bae, J.S. Kim, Z. Wang, J. Yan, Y. Zhuang, Y.M. Lee, Tröger's Base (TB)-containing polyimide membranes derived from bio-based dianhydrides for gas separations, J. Membr. Sci., 610 (2020) 118255. https://doi.org/10.1016/j.memsci.2020.118255

[11] J.G. Seong, Y. Zhuang, S. Kim, Y.S. Do, W.H. Lee, M.D. Guiver, Y.M. Lee, Effect of methanol treatment on gas sorption and transport behavior of intrinsically microporous polyimide membranes incorporating Tröger's base, J. Membr. Sci., 480 (2015) 104-114. https://doi.org/10.1016/j.memsci.2015.01.022

[12] D. Zhang, J.G. Seong, W.H. Lee, S. Ando, Y. Wan, Y.M. Lee, Y. Zhuang, Effects of sulfonate incorporation and structural isomerism on physical and gas transport properties of soluble sulfonated polyimides, Polymer, 191 (2020) 122263. https://doi.org/10.1016/j.polymer.2020.122263

[13] Y. Zhang, W.H. Lee, J.G. Seong, J.Y. Bae, Y. Zhuang, S. Feng, Y. Wan, Y.M. Lee, Alicyclic segments upgrade hydrogen separation performance of intrinsically microporous polyimide membranes, J. Membr. Sci., 611 (2020) 118363. https://doi.org/10.1016/j.memsci.2020.118363

[14] Y. Zhuang, J.G. Seong, Y.S. Do, W.H. Lee, M.J. Lee, Z. Cui, A.E. Lozano, M.D. Guiver, Y.M. Lee, Soluble, microporous, Troger's Base copolyimides with tunable membrane performance for gas separation, Chem. Commun., 52 (2016) 3817-3820. http://doi.org/10.1039/C5CC09783E

[15] Y. Zhuang, J.G. Seong, Y.S. Do, W.H. Lee, M.J. Lee, M.D. Guiver, Y.M. Lee, High-strength, soluble polyimide membranes incorporating Tröger's Base for gas separation, J. Membr. Sci., 504 (2016) 55-65. https://doi.org/10.1016/j.memsci.2015.12.057

[16] W.H. Lee, J.G. Seong, X. Hu, Y.M. Lee, Recent progress in microporous polymers from thermally rearranged polymers and polymers of intrinsic microporosity for membrane gas separation: Pushing performance limits and revisiting trade-off lines, J. Polym. Sci., 58 (2020) 2450-2466. https://doi.org/10.1002/pol.20200110

[17] S. Kim, J.G. Seong, Y.S. Do, Y.M. Lee, Gas sorption and transport in thermally rearranged polybenzoxazole membranes derived from polyhydroxylamides, J. Membr. Sci., 474 (2015) 122-131. https://doi.org/10.1016/j.memsci.2014.09.051

[18] D. Plaza-Lozano, B. Comesaña-Gándara, M. de la Viuda, J.G. Seong, L. Palacio, P. Prádanos, G. José, P. Cuadrado, Y.M. Lee, A. Hernández, New aromatic polyamides and polyimides having an adamantane bulky group, Mater. Today Commun., 5 (2015) 23-31. https://doi.org/10.1016/j.mtcomm.2015.10.001

[19] Y. Zhuang, J.G. Seong, Y.S. Do, H.J. Jo, Z. Cui, J. Lee, Y.M. Lee, M.D. Guiver, Intrinsically microporous soluble polyimides incorporating tröger's base for membrane gas separation, Macromolecules, 47 (2014) 3254-3262. https://doi.org/10.1021/ma5007073

[20] Y. Zhuang, J.G. Seong, Y.S. Do, H.J. Jo, M.J. Lee, G. Wang, M.D. Guiver, Y.M. Lee, Effect of isomerism on molecular packing and gas transport properties of poly (benzoxazole-co-imide) s, Macromolecules, 47 (2014) 7947-7957. https://doi.org/10.1021/ma501891m

[21] R.J. Plunkett, Tetrafluoroethylene polymers, United States patent, US No. 2,230,654 (1941).

[22] T.C. Merkel, I. Pinnau, R. Prabhakar, B.D. Freeman, Gas and vapor transport properties of perfluoropolymers, Materials science of membranes for gas and vapor separation, 1 (2006). https://doi.org/10.1002/047002903x

[23] Z. Cui, E. Drioli, Y.M. Lee, Recent progress in fluoropolymers for membranes, Prog. Polym. Sci., 39 (2014) 164-198. https://doi.org/10.1016/j.progpolymsci.2013.07.008

[24] Y. Okamoto, H. Zhang, F. Mikes, Y. Koike, Z. He, T.C. Merkel, New perfluoro-dioxolane-based membranes for gas separations, J. Membr. Sci., 471 (2014) 412-419. https://doi.org/10.1016/j.memsci.2014.07.074

[25] A.Y. Alentiev, V. Shantarovich, T. Merkel, V. Bondar, B. Freeman, Y.P. Yampolskii, Gas and vapor sorption, permeation, and diffusion in glassy amorphous Teflon AF1600, Macromolecules, 35 (2002) 9513-9522. https://doi.org/10.1021/ma020494f

[26] A.Y. Alentiev, Y.P. Yampolskii, V. Shantarovich, S. Nemser, N. Plate, High transport parameters and free volume of perfluorodioxole copolymers, J. Membr. Sci., 126 (1997) 123-132. https://doi.org/10.1016/S0376-7388(96)00272-4

[27] V. Bondar, B. Freeman, Y.P. Yampolskii, Sorption of gases and vapors in an amorphous glassy perfluorodioxole copolymer, Macromolecules, 32 (1999) 6163-6171. https://doi.org/10.1021/ma9817222

[28] T. Merkel, V. Bondar, K. Nagai, B. Freeman, Y.P. Yampolskii, Gas sorption, diffusion, and permeation in poly (2, 2-bis (trifluoromethyl)-4, 5-difluoro-1, 3-dioxole-co-tetrafluoroethylene), Macromolecules, 32 (1999) 8427-8440. https://doi.org/10.1021/ma990685r

[29] Y. Yampolskii, Polymeric Gas Separation Membranes, Macromolecules, 45 (2012) 3298-3311. https://doi.org/10.1021/ma300213b

[30] M. Hellums, W. Koros, G. Husk, D. Paul, Fluorinated polycarbonates for gas separation applications, J. Membr. Sci., 46 (1989) 93-112. https://doi.org/10.1016/S0376-7388(00)81173-4

[31] K. Tanaka, H. Kita, M. Okano, K.-i. Okamoto, Permeability and permselectivity of gases in fluorinated and non-fluorinated polyimides, Polymer, 33 (1992) 585-592. https://doi.org/10.1016/0032-3861(92)90736-G

[32] A.X. Wu, J.A. Drayton, K. Mizrahi Rodriguez, F.M. Benedetti, Q. Qian, S. Lin, Z.P. Smith, Elucidating the Role of Fluorine Content on Gas Sorption Properties of Fluorinated Polyimides, Macromolecules, 54 (2021) 22-34. https://doi.org/10.1021/acs.macromol.0c01746

[33] A. Fuoco, B. Satilmis, T. Uyar, M. Monteleone, E. Esposito, C. Muzzi, E. Tocci, M. Longo, M.P. De Santo, M. Lanč, Comparison of pure and mixed gas permeation of the highly fluorinated polymer of intrinsic microporosity PIM-2 under dry and humid conditions: Experiment and modelling, J. Membr. Sci., 594 (2020) 117460. https://doi.org/10.1016/j.memsci.2019.117460

[34] H.B. Park, C.H. Jung, Y.M. Lee, A.J. Hill, S.J. Pas, S.T. Mudie, E. Van Wagner, B.D. Freeman, D.J. Cookson, Polymers with cavities tuned for fast selective transport of small molecules and ions, Science, 318 (2007) 254-258. https://doi.org/10.1126/science.1146744

[35] S. Kim, Y.M. Lee, Rigid and microporous polymers for gas separation membranes, Prog. Polym. Sci., 43 (2015) 1-32. https://doi.org/10.1016/j.progpolymsci.2014.10.005

[36] G. Dong, Y.M. Lee, Microporous polymeric membranes inspired by adsorbent for gas separation, J. Mater. Chem. A, 5 (2017) 13294-13319. https://doi.org/10.1039/C7TA04015F

[37] Y.S. Do, J.G. Seong, S. Kim, J.G. Lee, Y.M. Lee, Thermally rearranged (TR) poly (benzoxazole-co-amide) membranes for hydrogen separation derived from 3, 3′-dihydroxy-4, 4′-diamino-biphenyl (HAB), 4, 4′-oxydianiline (ODA) and isophthaloyl chloride (IPCl), J. Membr. Sci., 446 (2013) 294-302. https://doi.org/10.1016/j.memsci.2013.06.059

[38] S.H. Han, H.J. Kwon, K.Y. Kim, J.G. Seong, C.H. Park, S. Kim, C.M. Doherty, A.W. Thornton, A.J. Hill, A.E. Lozano, Tuning microcavities in thermally rearranged polymer membranes for CO 2 capture, Phys. Chem. Chem. Phys., 14 (2012) 4365-4373. https://doi.org/10.1039/C2CP23729F

[39] S. Kim, J. Hou, Y. Wang, R. Ou, G.P. Simon, J.G. Seong, Y.M. Lee, H. Wang, Highly permeable thermally rearranged polymer composite membranes with a graphene oxide scaffold for gas separation, J. Mater. Chem. A, 6 (2018) 7668-7674. https://doi.org/10.1039/C8TA02256A

[40] Y. Wang, Z.X. Low, S. Kim, H. Zhang, X. Chen, J. Hou, J.G. Seong, Y.M. Lee, G.P. Simon, C.H. Davies, Functionalized boron nitride nanosheets: a thermally rearranged polymer nanocomposite membrane for hydrogen separation, Angew. Chem. Int. Ed., 130 (2018) 16288-16293. https://doi.org/10.1002/ange.201809126

[41] J. Lee, J.S. Kim, J.F. Kim, H.J. Jo, H. Park, J.G. Seong, Y.M. Lee, Densification-induced hollow fiber membranes using crosslinked thermally rearranged (XTR) polymer for CO2 capture, J. Membr. Sci., 573 (2019) 393-402. https://doi.org/10.1016/j.memsci.2018.12.023

[42] X. Hu, W.H. Lee, J. Zhao, J.S. Kim, Z. Wang, J. Yan, Y. Zhuang, Y.M. Lee, Thermally rearranged polymer membranes containing highly rigid biphenyl ortho-hydroxyl diamine for hydrogen separation, J. Membr. Sci., 604 (2020) 118053. https://doi.org/10.1016/j.memsci.2020.118053

[43] X. Hu, W.H. Lee, J.Y. Bae, J.S. Kim, J.T. Jung, H.H. Wang, H.J. Park, Y.M. Lee,

Thermally rearranged polybenzoxazole copolymers incorporating Tröger's base for high flux gas separation membranes, J. Membr. Sci., 612 (2020) 118437. https://doi.org/10.1016/j.memsci.2020.118437

[44] S.J.D. Smith, R. Hou, C.H. Lau, K. Konstas, M. Kitchin, G. Dong, J. Lee, W.H. Lee, J.G. Seong, Y.M. Lee, M.R. Hill, Highly permeable Thermally Rearranged Mixed Matrix Membranes (TR-MMM), J. Membr. Sci., 585 (2019) 260-270. https://doi.org/10.1016/j.memsci.2019.05.046

[45] S. Kim, E. Shamsaei, X. Lin, Y. Hu, G.P. Simon, J.G. Seong, J.S. Kim, W.H. Lee, Y.M. Lee, H. Wang, The enhanced hydrogen separation performance of mixed matrix membranes by incorporation of two-dimensional ZIF-L into polyimide containing hydroxyl group, J. Membr. Sci., 549 (2018) 260-266. https://doi.org/10.1016/j.memsci.2017.12.022

[46] Y. Zhuang, J.G. Seong, W.H. Lee, Y.S. Do, M.J. Lee, G. Wang, M.D. Guiver, Y.M. Lee, Mechanically Tough, Thermally Rearranged (TR) Random/Block Poly(benzoxazole-co-imide) Gas Separation Membranes, Macromolecules, 48 (2015) 5286-5299. https://doi.org/10.1021/acs.macromol.5b00930

[47] C. Aguilar-Lugo, W.H. Lee, J.A. Miguel, J.G. de la Campa, P. Prádanos, J.Y. Bae, Y.M. Lee, C. Álvarez, A.n.E. Lozano, Highly Permeable Mixed Matrix Membranes of Thermally Rearranged Polymers and Porous Polymer Networks for Gas Separations, ACS Appl. Polym. Mater., (2021). https://doi.org/10.1021/acsapm.1c01012

[48] Y. Lu, X. Hu, W.H. Lee, J.Y. Bae, J. Zhao, W. Nie, Z. Wang, J. Yan, Y.M. Lee, Effects of bulky 2, 2′-substituents in dianhydrides on the microstructures and gas transport properties of thermally rearranged polybenzoxazoles, J. Membr. Sci., 639 (2021) 119777. https://doi.org/10.1016/j.memsci.2021.119777

[49] W.H. Lee, J.Y. Bae, A. Yushkin, M. Efimov, J.T. Jung, A. Volkov, Y.M. Lee, Energy and time efficient infrared (IR) irradiation treatment for preparing thermally rearranged (TR) and carbon molecular sieve (CMS) membranes for gas separation, J. Membr. Sci., 613 (2020) 118477. https://doi.org/10.1016/j.memsci.2020.118477

[50] A. Brunetti, E. Tocci, M. Cersosimo, J.S. Kim, W.H. Lee, J.G. Seong, Y.M. Lee, E. Drioli, G. Barbieri, Mutual influence of mixed-gas permeation in thermally rearranged poly(benzoxazole-co-imide) polymer membranes, J. Membr. Sci., 580 (2019) 202-213. https://doi.org/10.1016/j.memsci.2019.01.058

[51] J.H. Lee, J. Lee, H.J. Jo, J.G. Seong, J.S. Kim, W.H. Lee, J. Moon, D. Lee, W.J. Oh, J.-g. Yeo, Y.M. Lee, Wet CO 2 /N 2 permeation through a crosslinked thermally rearranged poly(benzoxazole- co -imide) (XTR-PBOI) hollow fiber membrane module for CO 2 capture, J. Membr. Sci., 539 (2017) 412-420. https://doi.org/10.1016/j.memsci.2017.06.032

[52] K.T. Woo, G. Dong, J. Lee, J.S. Kim, Y.S. Do, W.H. Lee, H.S. Lee, Y.M. Lee, Ternary mixed-gas separation for flue gas CO2 capture using high performance thermally rearranged (TR) hollow fiber membranes, J. Membr. Sci., 510 (2016) 472-480. https://doi.org/10.1016/j.memsci.2016.03.033

[53] J.G. Seong, W.H. Lee, J. Lee, S.Y. Lee, Y.S. Do, J.Y. Bae, S.J. Moon, C.H. Park, H.J. Jo, J.S. Kim, K.-R. Lee, W.-S. Hung, J.-Y. Lai, Y. Ren, C.J. Roos, R.P. Lively, Y.M. Lee, Microporous polymers with cascaded cavities for controlled transport of small gas molecules, Sci. Adv., 7 (2021) eabi9062. http://doi.org/10.1126/sciadv.abi9062

[54] W.H. Lee, J.G. Seong, J.Y. Bae, H.H. Wang, S.J. Moon, J.T. Jung, Y.S. Do, H. Kang, C.H. Park, Y.M. Lee, Thermally rearranged semi-interpenetrating polymer network (TR-SIPN) membranes for gas and olefin/paraffin separation, J. Membr. Sci., 625 (2021) 119157. https://doi.org/10.1016/j.memsci.2021.119157

[55] Y.S. Do, W.H. Lee, J.G. Seong, J.S. Kim, H.H. Wang, C.M. Doherty, A.J. Hill, Y.M. Lee, Thermally rearranged (TR) bismaleimide-based network polymers for gas separation membranes, Chem. Commun., 52 (2016) 13556-13559. https://doi.org/10.1039/C6CC06609G

[56] C.A. Scholes, C.P. Ribeiro, S.E. Kentish, B.D. Freeman, Thermal rearranged poly(benzoxazole-co-imide) membranes for CO2 separation, J. Membr. Sci., 450 (2014) 72-80. https://doi.org/10.1016/j.memsci.2013.08.049

[57] Q. Liu, D.R. Paul, B.D. Freeman, Gas permeation and mechanical properties of thermally rearranged (TR) copolyimides, Polymer, 82 (2016) 378-391. https://doi.org/10.1016/j.polymer.2015.11.051

[58] C.A. Scholes, C.P. Ribeiro, S.E. Kentish, B.D. Freeman, Thermal rearranged poly(benzoxazole)/polyimide blended membranes for CO2 separation, Sep. Purif. Technol., 124 (2014) 134-140. https://doi.org/10.1016/j.seppur.2014.01.012

[59] A. Kushwaha, M.E. Dose, S. Luo, B.D. Freeman, R. Guo, Polybenzoxazole (PBO)-based gas separation membranes thermally derived from blends of Ortho-functional polyimide and polyamide precursors, Sep. Purif. Technol., 184 (2017) 384-393. https://doi.org/10.1016/j.seppur.2017.04.051

[60] J.D. Moon, A.T. Bridge, C. D'Ambra, B.D. Freeman, D.R. Paul, Gas separation properties of polybenzimidazole/thermally-rearranged polymer blends, J. Membr. Sci., 582 (2019) 182-193. https://doi.org/10.1016/j.memsci.2019.03.067

[61] W.F. Yong, H. Zhang, Recent advances in polymer blend membranes for gas separation and pervaporation, Prog. Mater. Sci., 116 (2021) 100713. https://doi.org/10.1016/j.pmatsci.2020.100713

[62] S.J. Moon, J.H. Kim, J.G. Seong, W.H. Lee, S.H. Park, S.H. Noh, J.H. Kim, Y.M. Lee, Thin film composite on fluorinated thermally rearranged polymer nanofibrous membrane achieves power density of 87 W m−2 in pressure retarded osmosis, improving economics of osmotic heat engine, J. Membr. Sci., 607 (2020) 118120. https://doi.org/10.1016/j.memsci.2020.118120

[63] N. Chen, C. Hu, H.H. Wang, S.P. Kim, H.M. Kim, W.H. Lee, J.Y. Bae, J.H. Park, Y.M. Lee, Poly(Alkyl-Terphenyl Piperidinium) Ionomers and Membranes with an Outstanding Alkaline-Membrane Fuel-Cell Performance of 2.58 W cm-2, Angew. Chem. Int. Ed. 60 (2021) 7710-7718. https://doi.org/10.1002/ange.202013395

[64] N. Chen, H.H. Wang, S.P. Kim, H.M. Kim, W.H. Lee, C. Hu, J.Y. Bae, E.S. Sim, Y.C. Chung, J.H. Jang, S.J. Yoo, Y. Zhuang, Y.M. Lee, Poly(fluorenyl aryl piperidinium) membranes and ionomers for anion exchange membrane fuel cells, Nat. Commun., 12 (2021) 2367. https://doi.org/10.1038/s41467-021-22612-3

[65] A.C. Comer, C.P. Ribeiro, B.D. Freeman, S. Kalakkunnath, D.S. Kalika, Dynamic relaxation characteristics of thermally rearranged aromatic polyimides, Polymer, 54 (2013) 891-900. https://doi.org/10.1016/j.polymer.2012.12.022

[66] A.K. Padhan, D. Mandal, Thermo-reversible self-healing in a fluorous crosslinked copolymer, Polym. Chem., 9 (2018) 3248-3261. https://doi.org/10.1039/C8PY00471D

[67] S.H. Han, N. Misdan, S. Kim, C.M. Doherty, A.J. Hill, Y.M. Lee, Thermally rearranged (TR) polybenzoxazole: effects of diverse imidization routes on physical properties and gas transport behaviors, Macromolecules, 43 (2010) 7657-7667. https://doi.org/10.1021/ma101549z

[68] C.A. Scholes, C.P. Ribeiro, S.E. Kentish, B.D. Freeman, Thermal rearranged poly (benzoxazole)/polyimide blended membranes for CO2 separation, Sep. Puri. Tech., 124 (2014) 134-140. https://doi.org/10.1016/j.seppur.2014.01.012

[69] C.A. Scholes, C.P. Ribeiro, S.E. Kentish, B.D. Freeman, Thermal rearranged poly (benzoxazole-co-imide) membranes for CO2 separation, J. Membr. Sci., 450 (2014) 72-80. https://doi.org/10.1016/j.memsci.2013.08.049

[70] C.A. Scholes, Thermally rearranged poly (benzoxazole) copolymer membranes for improved gas separation: a review, Aust. J. Chem., 69 (2016) 601-611. https://doi.org/10.1071/CH15523

[71] L.M. Robeson, Correlation of separation factor versus permeability for polymeric membranes, J. Membr. Sci., 62 (1991) 165-185. https://doi.org/10.1016/0376-7388(91)80060-J

[72] B. Comesaña-Gándara, J. Chen, C.G. Bezzu, M. Carta, I. Rose, M.-C. Ferrari, E. Esposito, A. Fuoco, J.C. Jansen, N.B. McKeown, Redefining the Robeson upper bounds for CO 2/CH 4 and CO 2/N 2 separations using a series of ultrapermeable benzotriptycene-based polymers of intrinsic microporosity, Energy Environ. Sci., 12 (2019) 2733-2740. https://doi.org/10.1039/C9EE01384A

[73] R. Swaidan, B. Ghanem, I. Pinnau, Fine-tuned intrinsically ultramicroporous polymers redefine the permeability/selectivity upper bounds of membrane-based air and hydrogen separations, ACS Macro Lett., 4(9) (2015) 947-951. https://doi.org/10.1021/acsmacrolett.5b00512

[74] S. Bandehali, A.E. Amooghin, H. Sanaeepur, R. Ahmadi, A. Fuoco, J.C. Jansen, S. Shirazian, Polymers of Intrinsic Microporosity and Thermally Rearranged Polymer Membranes for Highly Efficient Gas Separation, Sep. Puri. Tech., 278 (2021) 119513. https://doi.org/10.1016/j.seppur.2021.119513